



UNIVERSITY OF LEEDS

This is a repository copy of *Design and operation of a Rayleigh Ohnesorge Jetting Extensional Rheometer (ROJER) to study extensional properties of low viscosity polymer solutions*.

White Rose Research Online URL for this paper:  
<http://eprints.whiterose.ac.uk/113583/>

Version: Accepted Version

---

**Article:**

Greiciunas, E, Wong, J, Gorbatenko, I et al. (6 more authors) (2017) Design and operation of a Rayleigh Ohnesorge Jetting Extensional Rheometer (ROJER) to study extensional properties of low viscosity polymer solutions. *Journal of Rheology*, 61 (3). ISSN 0148-6055

<https://doi.org/10.1122/1.4979099>

---

© 2017 The Author(s). This article may be downloaded for personal use only. Any other use requires prior permission of the author and AIP Publishing. The following article has been published by *Journal of Rheology*. It will be found at <https://doi.org/10.1122/1.4979099>. Uploaded in accordance with the publisher's self-archiving policy.

**Reuse**

Unless indicated otherwise, fulltext items are protected by copyright with all rights reserved. The copyright exception in section 29 of the Copyright, Designs and Patents Act 1988 allows the making of a single copy solely for the purpose of non-commercial research or private study within the limits of fair dealing. The publisher or other rights-holder may allow further reproduction and re-use of this version - refer to the White Rose Research Online record for this item. Where records identify the publisher as the copyright holder, users can verify any specific terms of use on the publisher's website.

**Takedown**

If you consider content in White Rose Research Online to be in breach of UK law, please notify us by emailing [eprints@whiterose.ac.uk](mailto:eprints@whiterose.ac.uk) including the URL of the record and the reason for the withdrawal request.



[eprints@whiterose.ac.uk](mailto:eprints@whiterose.ac.uk)  
<https://eprints.whiterose.ac.uk/>

# **Design and operation of a Rayleigh Ohnesorge Jetting Extensional Rheometer (ROJER) to study extensional properties of low viscosity polymer solutions**

E.Greiciunas,\* J.Wong,\* I.Gorbatenko,\* J. Hall,\* M.C.T. Wilson, N. Kapur,<sup>†</sup> and O.G. Harlen<sup>‡</sup>  
*University of Leeds, Leeds LS2 9JT, United Kingdom*

D. Vadillo

*AkzoNobel Surface Chemistry, LLC., 10 Finderne Avenue,  
Suite A, Bridgewater, New Jersey, 08807*

P. Threlfall-Holmes<sup>†</sup>

*TH Collaborative Innovation, Belmont Vicarage,  
Broomside Lane, Durham, DH1 2QW, United Kingdom and  
University of Leeds, Leeds LS2 9JT, United Kingdom*

(Dated: March 8, 2017)

## **Abstract**

The Rayleigh Ohnesorge Jetting Extensional Rheometer (ROJER) enables measurement of very short relaxation times of low viscosity complex fluids such as those encountered in ink-jet printing and spraying applications. This paper focuses on the design and operation of the ROJER. The performance of two nozzle designs are compared using Newtonian fluids alongside a study using computational fluid dynamics (CFD). Subsequently a disposable nozzle is developed that overcomes issues of blockage and cleaning. The operability of this design is subject to a focused study where low viscosity polymer solutions are characterised. The test fluid materials are ethyl hydroxy-ethyl cellulose (EHEC) and poly ethylene oxide (PEO) mixed with water/glycerol solutions. Results obtained by the disposable nozzle are encouraging, paving the way for a more cost-efficient and robust ROJER setup.

---

\* EPSRC Centre for Doctoral Training in Fluid Dynamics

<sup>†</sup> School of Mechanical Engineering

<sup>‡</sup> Author to whom correspondence should be addressed; electronic mail: O.G.Harlen@leeds.ac.uk; Department of Applied Mathematics

## I. INTRODUCTION

Characterisation of low viscosity polymeric fluids is important to an array of industries. In particular, highly extensional deformations are encountered in processes such as inkjet printing and spray coatings. Polymer additives are known to influence the stability and dynamics of capillary driven jet break-up. A classic example is the use of formulated inks designed to inhibit undesirable ‘satellite’ drops in the inkjet printing industry [1].

To control such applications, it is desirable to characterise the extensional rheology of the fluid. Whilst for a Newtonian fluid the extensional viscosity is simply three times its shear viscosity [2], for polymer solutions this ratio can be orders of magnitude greater owing to the additional resistance caused by polymer coils unravelling in strong extensional flows. Moreover a steady state is only achieved at very high strains, so the unravelling is a transient response that is characterised by the extensional relaxation time,  $\tau_E$ . In a range of practical applications extensional flows dominate the response of many materials and hence is of great interest to study [3].

Measuring extensional rheology has proven to be difficult for low viscosity polymer solutions. Only a limited number of geometries exist where a uniform extensional deformation with a high strain rate can be imposed, and measuring the forces directly is difficult. To date, the principle method measures the capillary thinning of a liquid bridge in an apparatus originally proposed by Bazilevsky et al. [4] commercialised as the Capillary Break-up Extensional Rheometer (CaBER). In this instrument a fluid sample is held between two plates that are suddenly separated to form a liquid bridge between them. The minimum bridge radius is then measured as it thins and breaks over a short period of time. The CaBER can probe relaxation times,  $\tau_E$ , of dilute polymer solutions in the range of 0.01 to 1 seconds [4]. However, the extension rates are constrained by the diameter of the endplates with a standard size being six millimetres. This dictates the characteristic length-scale in the definition of the Ohnesorge and Deborah numbers. The Ohnesorge number measures the relative magnitudes of the viscous and inertial forces during capillary thinning and is defined as

$$Oh = \frac{\mu\sqrt{2}}{\sqrt{\rho\sigma D_0}}, \quad (1)$$

where  $\mu$  is the shear viscosity,  $\rho$  is the density,  $\sigma$  is the surface tension and  $D_0$  is the initial diameter of the liquid bridge. The Deborah number is defined as

$$De = \frac{\tau_E}{t_D}, \quad (2)$$

where  $\tau_E$  is the relaxation time and  $t_D = \sqrt{\rho D_0^3 / 8\sigma}$  is the inertial (or Rayleigh) capillary time scale. At lower Deborah numbers a fluid behaves similarly to a Newtonian fluid whereas at a higher Deborah number, the thinning is dominated by fluid elasticity. The CaBER technique is further constrained by the plate separation time, which takes a minimum of 50 milliseconds in the commercial CaBER. The technique requires that the liquid bridge exists at the cessation of the separation step. Rodd et al. [5] showed that the standard CaBER technique fails if either the Ohnesorge or Deborah numbers are less than unity. This failure is associated with the fluid losing cohesion at the end plates or the fluid filament necking too rapidly.

Industrial applications require devices that can measure lower relaxation times of dilute solutions than those currently achieved by the commercial CaBER. Several authors have attempted to address this limitation. The Cambridge Trimaster, introduced by Vadillo et al. [6], is a modified capillary break-up apparatus. This has smaller diameter plates and much greater plate acceleration. Extensional relaxation times as low as 80 microseconds have been measured reliably using this device, although not for a fluid with a shear viscosity below 10 millipascal-seconds [7]. However, it is yet to be reported what combination of relaxation time and viscosity can reliably be achieved in practice. Regardless of the mechanical improvements to capillary break-up apparatus, a fundamental physical limit in lower viscosity fluids is the increasing influence of fluid inertia. It is no longer possible to make the simplifying assumption of a solely visco-capillary balance used in CaBER [8] and it is necessary to use a modified inertia-visco-capillary balance [9, 10]. To avoid the problem of fluid inertia, Campo-Deano and Clasen [11] developed the Slow Retraction Method (SRM). The experiment is performed using the CaBER hardware, but rather than imposing a rapid step strain on the fluid to create a liquid bridge beyond the point of necking instability, the fluid is very slowly separated to the point where rapid visco-capillary necking occurs. Whilst it avoids the fluid inertia problem, the SRM shares the need for a high-specification, high speed camera together with the necessary capillary thinning techniques and the skill to perform the experiment and analyse the data. These inherent costs and difficulties preclude widespread adoption of these techniques in practical industrial application.

An alternative approach that can potentially overcome these restrictions is the Rayleigh Ohnesorge Jetting Extensional Rheometer (ROJER), a relatively new technique developed by McKinley and colleagues [12, 13] that measures the thinning liquid bridges of a continuous jet. The most significant advantage of the ROJER over CaBER is the reduction in the characteristic length scale,

without the complication of imparted fluid inertia. This is the key modification in the ROJER that allows access to higher strain rates and hence much shorter relaxation times of low viscosity polymeric fluids. A key practical advantage is that by employing stroboscopic imaging, a conventional low speed camera can be used, with two orders of magnitude saving in imaging hardware cost. The ROJER remains a relatively new apparatus and much work remains to be done to fully explore its operability. A key enabling step to more widespread deployment of the ROJER is the development of a robust and simple mechanical setup and a tool to post-process experimental data.

During the ROJER experiment, fluid is jetted through a small diameter nozzle where a small perturbation is applied to drive capillary instability down the liquid jet. Within the jet, capillary stresses are resisted by inertial or viscous forces. For polymeric fluids, this can also be resisted by viscoelastic stresses. The instability eventually grows large enough to cause the jet to break up into droplets downstream. Provided that the jet velocity  $v_0$  is sufficiently high so that the Weber number

$$We = \frac{\rho v_0^2 D_0}{\sigma}, \quad (3)$$

is large, the initial stages of instability viewed in a frame moving with the fluid velocity are equivalent to those of an infinite jet [14], so that in the initial phase of the disturbance the minimum jet diameter decays according to

$$\frac{D(t)}{D_0} = 1 - \delta \exp(\alpha t), \quad (4)$$

where  $D(t)$  is the minimum jet diameter over time,  $\delta$  is the initial perturbation amplitude and  $\alpha$  is the growth rate of the instability [15]. Following Rayleigh's classical linear stability analysis, the fastest growing mode is achieved at a critical wavelength of  $\lambda^* \approx 4.5D_0$  for an inviscid fluid. Once the jet approaches break-up, non-linear effects begin to dominate fluid behaviour. The break-off event represents a singularity in the continuum equations. For Newtonian fluids the approach to pinch off can be captured mathematically by one of a number of similarity solutions, which depend upon the Ohnesorge number [16].

Incorporation of viscoelastic effects into the linear stability analysis was completed by Middleman [17] who found that the viscoelasticity promotes instability in the linear regime. Unravelling of polymer chains in the non-linear regime resists capillary thinning, increasing the jet break-up length and time to break-up. In this elasto-capillary thinning regime, viscoelastic stresses become the dominant force resisting the capillary pressure. It has been shown both theoretically

and experimentally that on approach to pinch off the filament thins exponentially [3, 18], and for the Oldroyd-B model, Clasen et al. [19] (correcting earlier work [20]) showed that the thinning diameter of a jet in the elasto-capillary regime decays as

$$\frac{D(t)}{D_0} = (GD_0/4\sigma)^{1/3} \exp(-t/3\tau_E). \quad (5)$$

where  $D_0$  is the initial jet diameter and  $G$  is the elastic modulus. From the evolution of the thinning filament diameter,  $D(t)$ , the instantaneous strain rate  $\dot{\epsilon}$  is given by

$$\dot{\epsilon} = \frac{2}{D(t)} \frac{dD(t)}{dt}, \quad (6)$$

and becomes equal to  $2/(3\tau_E)$  in the elasto-capillary regime [3]. The elasto-capillary regime ends once the polymers approach their maximum extensibility, and their contribution to the extensional viscosity plateaus and the filament breaks up.

The scope of this paper is to investigate the design and operation of the ROJER. Newtonian water-glycerol solutions are used to validate the ROJER as an extensional rheometer by comparing experimental measurements to both theory and computational fluid dynamics simulations. These tests are used to compare the performance of two different nozzle designs: one using an orifice from an electron microscope and the other a disposable needle, which allows a more practical design for routine operation. A small study tested the use of different waveforms to drive the perturbations. Ethyl hydroxy-ethyl cellulose (EHEC) and poly-ethylene oxide (PEO) solutions are characterised at various polymer concentrations using the ROJER. The results obtained are compared to the theory and experimental results available in the literature. The data obtained by the ROJER are then compared against data obtained using the CaBER technique for the same polymeric solutions.

## II. METHODOLOGY

### A. Experimental Apparatus

A schematic of the experimental apparatus is presented in Figure 1. The ROJER setup used was substantially similar to the designs by Sharma et al. [13] and Keshavarz et al. [12]. However, rather than using a stroboscopic technique a high speed camera was used in order to observe the real-time break-up behaviour of particular sections of the jet. The apparatus enables control over jet break-up by imposing a perturbation of amplitude  $\delta$  and frequency  $f$ , specified using the

function generator (TTi TGA-12100), through piezoelectric transducers at the nozzle. The fluid is pumped through the nozzle at a constant volumetric flow rate using a syringe pump (Harvard Apparatus PHD ULTRA-4400). A custom made collimated LED light source is used to backlight the fluid. Evolution of the thinning fluid neck diameter,  $D(t)$ , is visualised using a high-speed

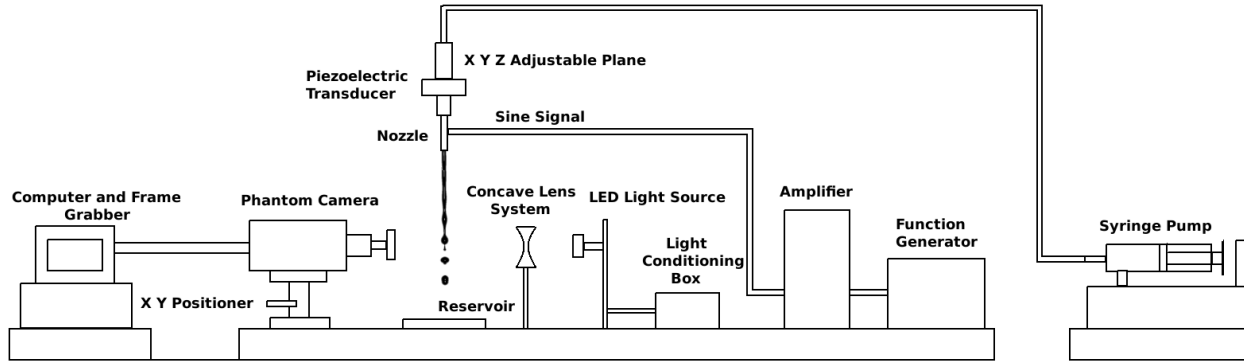


FIG. 1. A schematic diagram of the ROJER setup

camera (Vision Research Phantom 5089 V7) coupled to a high magnification lens (Navitar Zoom 6000). Typically in the experiments, the camera captured up to 24,096 frames per second with a resolution of  $800 \times 104$  pixels and an exposure time of 3 microseconds, at a magnification where the lens optical resolution and camera pixel resolution were both approximately 8 micrometres. Collected videos of the jet were stored as multi-page TIFF files to preserve image quality for post-processing.

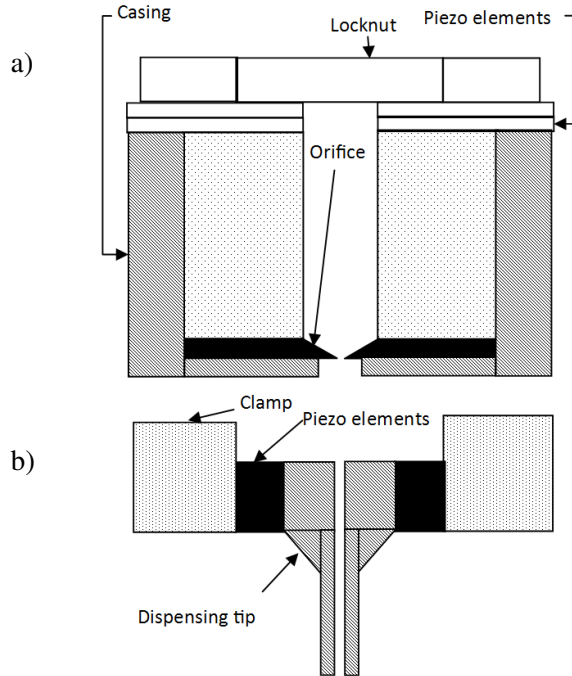


FIG. 2. The two test nozzle designs: (a) the orifice design that forms a uniform velocity profile at the nozzle exit, (b) the needle design that forms a parabolic velocity profile at the nozzle exit.

### 1. Nozzle designs

Two different nozzles are evaluated. The first (Figure 2a) was custom made for the ROJER by TTP PLC, and uses an electron microscope aperture (Agar Scientific AGA0211P) for the orifice of diameter  $200\mu\text{m}$ . This nozzle is used to characterise Newtonian fluids. In the orifice design, the perturbation is applied in an axial direction above the exit using a cylindrical stack of annular piezoelectric transducers. Though the nozzle stack is effective at driving a disturbance, the mechanical containment needed to support such a small thin plate aperture is time consuming to disassemble for cleaning or replacement. The nozzle also necessitates a recessed orifice, which in operation is prone to wetting-out and dripping. Regardless of the specific geometry any small diameter nozzle is prone to blockage, which is especially encountered when testing industrial fluid samples and generally requires disassembly and possibly replacement. The parts and labour costs associated with this means that this nozzle design is undesirable for industrial use, preventing widespread deployment of the ROJER as a commercial apparatus.

To circumvent these operational issues, a second nozzle design was constructed (Figure 2b). This design consists of a disposable stainless steel hypodermic needle tip, with an inner diameter

TABLE I. Physical properties of the Newtonian test fluids

Glycerol (wt. %)	$\rho$ (kg/m <sup>3</sup> )	$\mu_s$ (mPa · s)	$\sigma$ (mN/m)
0%	1,000	1.0	73.5
40%	1,153	6.7	62.0
74%	1,172	35.8	62.0

of  $210\mu\text{m}$ , clamped between two piezoelectric chips (Thor Labs TA0505D024WB) and positioned symmetrically against the needle hub. Whereas the original nozzle is effectively an orifice plate giving a uniform flow profile across the jet, the needle design gives a parabolic velocity profile and so allows comparison of the effects of different flow profiles. Preliminary experiments showed that the high pressure drop experienced in the needle caused the motor syringe pump to stall, and the length of the needle vibrated in a transverse plane under the action of the piezoelectric elements and flow. To overcome this, the needle was shortened using a laser microjet cutter, but was kept sufficiently long so that a fully developed flow at the nozzle was ensured (following Durst et al. [21]) to aid comparison with the flow simulations.

## 2. Fluid Materials

A range of Newtonian fluids composed of water and water-glycerol solutions were used to test the two nozzle designs. In addition, a set of polymeric solutions were prepared in a range of concentrations of ethyl hydroxy-ethyl cellulose (EHEC), with molecular weight  $M_w \approx 2.5 \times 10^5$  kg/kmol, and poly-ethylene oxide (PEO), with molecular weight  $M_w \approx 3 \times 10^5$  kg/kmol. The polymers are mixed in a 25%/75% (by weight) glycerol/water solution. Shear viscosity,  $\mu_s$ , was measured with a conventional cone and plate rheometer (Malvern Kinexus) for all of the solutions at a variety of shear rates, ranging from 20 to 60 s<sup>-1</sup>. All polymeric fluid experiments are carried out within a week of preparation to minimise the possible effects of ageing and bacterial growth. Physical properties of the fluid materials are presented in Tables I and II for Newtonian and polymeric fluids respectively. All of the experiments are performed at a room temperature of 21°C ( $\pm 1^\circ\text{C}$ ).

Levels of dilution are determined by calculating ratios of  $c/c^*$ , where  $c$  is the polymer concen-

tration and  $c^*$  is the critical overlap concentration defined by,

$$c^* = \frac{0.77}{[\mu]}, \quad (7)$$

where  $[\mu]$  is the intrinsic viscosity [22]. In the case where  $c/c^* \ll 1$ , interactions between neighbouring molecules in the coiled state are negligible and a Rouse–Zimm description of a dilute polymer solution is valid. However in flows where the polymers become highly extended, interactions between molecules are important even at concentrations well below  $c^*$  [23].

## B. Experimental Method

The syringe pump flow-rate is set to  $Q = 5 \text{ ml/min}$ , producing a jet of sufficiently high Weber number ( $We \approx 20$ ) to approximate infinite jet break-up. The critical wavenumber  $k^*$  corresponding to the fastest growth rate  $\alpha^*$  of the disturbance is then empirically determined to give the most stable break-up, since the fastest growing mode coincides with the shortest break-up length. For Newtonian fluids the critical frequency was selected using the linearised dispersion relation of a viscous jet [16], given by

$$\alpha^2 + \frac{3\mu k^2}{\rho} - \frac{\sigma k^2}{\rho D_0} \left(1 - \frac{k^2 D_0^2}{4}\right) = 0. \quad (8)$$

For polymeric fluids, a series of short videos were taken of the jet perturbed at different frequencies at intervals of 0.1 kHz, starting at the critical frequency of the water–glycerol solvent. From these videos, the critical frequency giving the shortest break–up length was established. A longer sequence was then recorded at this critical frequency, giving more break-up events for subsequent processing. For all of the experiments, the operating frequency ranged from 0.5 to 12 kHz. The perturbation amplitude was adjusted to the minimum required to ensure stable jet break-up. It was found that a larger drive amplitude was required for fluids with increasing viscosity and polymer loading due to additional viscoelastic resistance to break-up.

### 1. Post Processing

Greyscale images captured by the high-speed camera were converted to binary images by setting a threshold pixel value, which is selected by inspection and applied to all frames. Evolution of

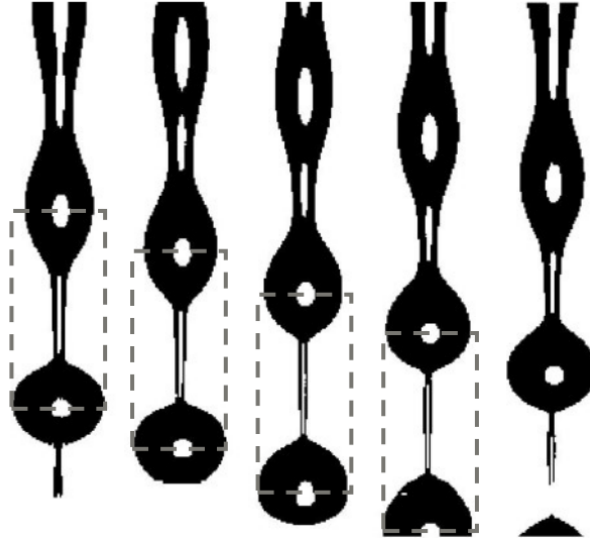


FIG. 3. A visualisation of the moving Lagrangian element (grey box) used to track the minimum filament diameter  $D(t)$ . The original greyscale has been converted to a binary image.

the thinning jet diameter  $D(t)$  is determined by tracking a Lagrangian window travelling at the jet velocity  $v_0$  (shown by the grey box in Figure 3) using a custom image analysis code, implemented in MATLAB. A typical video comprises of over 16,000 frames with four necks per frame, so there are potentially over 64,000 thinning necks as data points. The jet velocity relative to the camera frame rate typically gives 25–30 images for each individual liquid bridge as it passes through the imaging field of view giving in total approximately 2,000–3,000 Lagrangian fluid thinning bridges from each video. This abundance of data obtained by the ROJER allows a relatively simple algorithm to be used in the image analysis. The principle simplification employed is to measure the break-up of a single fluid neck in a Lagrangian window travelling at the jet velocity from the top of the image down to to break-up. Once a break-up event is detected within the Lagrangian window, the window repositions itself at the top of the image and tracks a new thinning neck. Using this algorithm approximately 500-600 necking events were observed in each video. Whilst this is considerably less than the potential 2,000-3,000 available it is still a sufficiently large sample to provide reliable averaging of the filament diameter measurements (as a check an analysis using only half the images produced identical results). In this respect ROJER has a significant advantage over CaBER in providing a large number of measurements of the thinning jet diameter  $D(t)$  within a single experiment, whereas CaBER is only able to provide one measurement of  $D(t)$  per experiment. The evolution of 500-600 thinning liquid bridges are super-imposed to form an

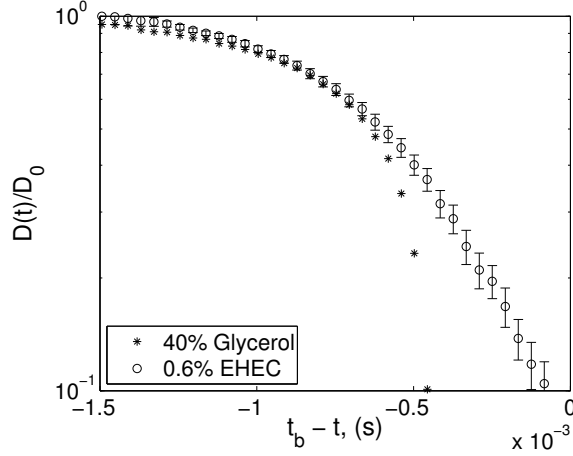


FIG. 4. A comparison of 40% glycerol Newtonian fluid ( $\star$ ) and the 0.6 % EHEC ( $\circ$ ) thinning curves. Newtonian fluid result was time shifted according to the longest break-up time.

averaged thinning curve, by setting the break-up time,  $t_b$  at a common zero to produce a negative time axis,  $t_b - t$ . Measurements at each point in time were then averaged to obtain  $D(t)$  together with the standard error,  $SE$ , given by

$$SE = \frac{\sqrt{\frac{1}{n} \sum_{i=1}^n (D_i - D)^2}}{\sqrt{n}} \quad (9)$$

where  $n$  is the number of observations,  $D_i$  at each time-point used to produce  $D(t)$ . An example of a filament thinning curve  $D(t)$ , together with the standard error  $SE$  obtained from the image analysis, is illustrated in Figure 4.

Figure 4 compares the thinning behaviour of a Newtonian 40% glycerol in water solution and a 0.6% EHEC in 25% glycerol/water solution. Both fluids show a similar initial growth rate of the perturbation but show quite different thinning behaviour approaching break-up. The thinning curve of the polymeric fluid deviates from that of the Newtonian fluid and subsequently is observed to decrease exponentially following a straight line on a semi-log plot as predicted by Equation 5. The relaxation time,  $\tau_E$ . was obtained by data regression of the data points in the elastocapillary regime (selected by visual inspection) in Figures 4 and subsequent figures.

### C. Computational Fluid Dynamics

ANSYS Fluent was used to simulate capillary driven jet break-up for Newtonian fluids, in order to validate the redesigned nozzle described in Section II A. The jet was modelled using a two dimensional axisymmetric geometry, shown to be a reasonable assumption for a jet perturbed at low amplitudes [24]. The evolution of the surface was captured using the Volume of Fluid (VOF) method, which tracks a volume of fluid in each cell of the mesh using the continuity equation. This numerical technique is a recommended model for modelling liquid-gas interactions in multiphase flows of this nature [25].

An explicit numerical scheme is implemented. The interface is reconstructed using geo-reconstruct, which utilises a piece-wise linear approach. Iterative time stepping increased solution stability and a time step of  $1 \times 10^{-8}$  s was used. A velocity perturbation driving the jet was implemented as a user defined function, given by

$$v = v_0 (1 + \delta \sin(2\pi ft)), \quad (10)$$

where  $v_0$  is the initial jet velocity,  $\delta$  is the amplitude of the disturbance and  $f$  is the frequency.

Since the thickness of the orifice plate is short compared to the length required for the flow to become fully established, a flat velocity profile was specified as the inlet condition, whereas a fully developed parabolic velocity profile was used for simulating the needle design. The flow rate of  $Q = 5$  ml/min was matched to that of the experiment. Cells of  $0.02D_0$  height and  $0.04D_0$  width across the liquid gas interface were used to create a graded mesh decreasing in resolution away from the interface. This minimised numerical diffusion at the interface and achieved mesh independence. All outer boundary conditions for the gas medium are specified as pressure outlets. Surface position data from the CFD was post-processed, using the same image analysis program described in Section II B 1, to determine the evolution of the thinning filament diameter  $D(t)$ .

## III. RESULTS I: ANALYSIS OF THE MECHANICAL DESIGN

### A. Nozzle Design

Newtonian experiments for the orifice design (Figure 2a) and the needle design (Figure 2b), which has a parabolic profile, were compared to CFD simulations and literature results.

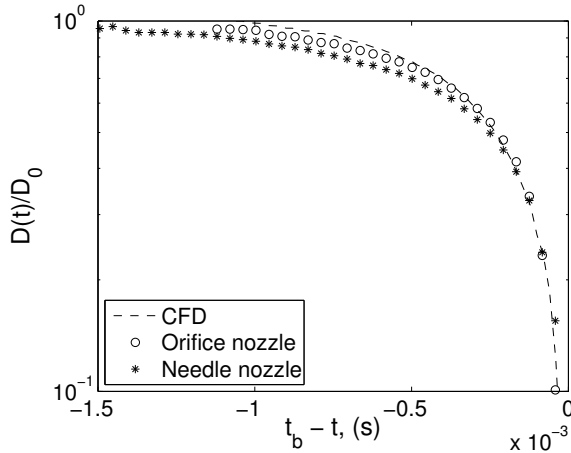


FIG. 5. A comparison of filament thinning using the orifice design ( $\circ$ ) and the needle design ( $*$ ) using a Newtonian 40% glycerol mixture. The black dashed line is the CFD result for the orifice nozzle. The orifice nozzle applied a perturbation at a frequency of 2.45 kHz, and the needle nozzle applied a perturbation at a frequency of 2.90 kHz ( $We = 22$ ,  $Oh = 0.0556$ ,  $Re = 84$ ).

At high Reynolds numbers the relaxation of the parabolic velocity profile outside the nozzle causes the jet to contract as it leaves the nozzle in order to conserve mass and momentum. In practice the extent of this contraction depends on the flow Reynolds number [26], with a jet at  $Re \simeq 100$  contracting to 0.87 of the nozzle diameter. This contraction must be taken into account when determining the critical frequency corresponding to the shortest break-up length. For Newtonian fluids the critical frequency increased by approximately 0.5 – 1 kHz compared to the critical computed from Equation 8, and by more for viscoelastic fluids when using the needle design. Figure 5 shows the output for both nozzles, where the critical frequency for the needle design has been adjusted to account for the jet contraction, together with results from the CFD. Strong agreement is found between all, showing that given the correct adjustments, the results for the needle and orifice nozzle are equivalent for Newtonian fluids. Figure 6 compares the calculated and observed jet shapes for the 74% glycerol solution.

## B. Perturbation functions

The function generator is used to test whether sine or square wave signals driving the perturbations affect the experimental results. This was checked using the 1.0% EHEC solution. The

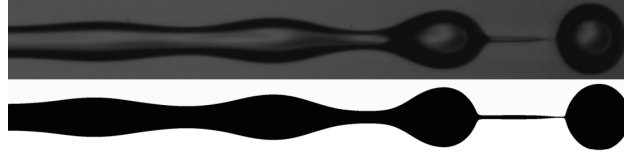


FIG. 6. A comparison of a video snapshot from the ROJER experiment (above) and the CFD result (below) using a 74% glycerol solution ( $We = 17.4, Oh = 0.293$ ).

thinning curves  $D(t)$  for both the sine and square waves are presented in Figure 7. Both data sets show a small oscillation which we believe is associated with the data acquisition process as we do not use sub-pixel resolution. The relaxation times measured are  $343 \mu s$  and  $328 \mu s$  for the sine and square waves respectively. This suggests that the perturbation function form is not important provided that the perturbation amplitude applied to the jet is small. This is of practical importance, since a simple square wave pulse generator can be used to provide the drive signal and a waveform generator is not required. Furthermore the piezoelectric actuators run cooler with a square wave drive, which makes the mechanical design of the needle nozzle clamp simpler and more reliable in operation.

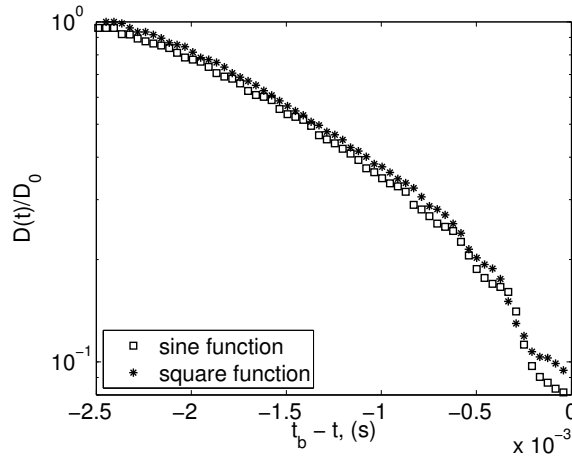


FIG. 7. Filament thinning curves of 1% EHEC solutions using (\*) - square and (□) - sine perturbation functions.

TABLE II. Relaxation times,  $\tau_E$ , observed using the ROJER together with the physical properties of various concentrations of EHEC and PEO. The density was  $\rho = 1,045 \text{ kg/m}^3$  and surface tension was  $\sigma = 62 \text{ mN/m}$  throughout. All concentrations of EHEC and PEO are mixed in a solvent of 25 % glycerol/ 75 % water.

Polymer wt. %	$\mu$ (mPa · s)	$c/c^*$	$\tau_E$ ( $\mu\text{s}$ )	$SE$ ( $\mu\text{s}$ )	$De$
EHEC 0.4%	7.8	2.08	139	8	0.4
EHEC 0.6%	11.5	3.12	139	6	0.3
EHEC 0.8%	20.7	4.16	309	8	0.8
EHEC 1.0%	28.0	5.20	343	6	0.9
PEO 0.025%	2.9	0.09	102	2	0.3
PEO 0.05%	2.9	0.19	165	2	0.4
PEO 0.1%	3.5	0.38	233	5	0.6

#### IV. RESULTS II: CHARACTERISATION OF EHEC AND PEO

A range of different polymer concentrations of EHEC and PEO are tested to measure their extensional properties and explore the limits of the mechanical setup. Results are given in Table II. Two lower EHEC concentration of 0.1 % and 0.2 % were also studied for which we were not able to observe elastocapillary thinning. Thinning curves of EHEC at concentrations between 0.4 % and 1.0 % are shown in Figure 8. The curve-fitting procedure, described in Section II B 1, determined relaxation times ranging from 139 to 343  $\mu\text{s}$ .

In contrast to the EHEC solutions, a principle limitation of the PEO solutions is that the two highest concentrations (0.2 % and 0.4 %) produced liquid bridges that decayed too slowly for the thinning regimes to be wholly captured within the camera field of view. The thinning curves of PEO at concentrations between 0.025 % and 0.1 % are shown in Figure 9. Over the range of concentrations tested, the fluid relaxation time was between 102 and 233  $\mu\text{s}$ . These results can be compared to relaxation times obtained by Keshavarz et al. [12] using a similar ROJER apparatus. Keshavarz et al. [12] observed a relaxation time of  $\tau_E = 360 \mu\text{s}$  for a 0.1% concentration of the same molecular weight ( $M_w \approx 3 \times 10^5 \text{ kg/kmol}$ ), but in a 40% glycerol in water, compared to the

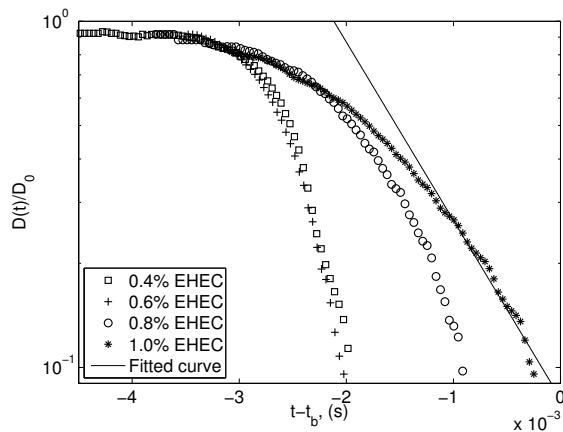


FIG. 8. The EHEC filament thinning curve as a function of time,  $D(t)$ . ( $\square$ ) - 0.4 % EHEC, ( $+$ ) - 0.6 % EHEC, ( $\circ$ ) - 0.8 % EHEC, ( $*$ ) - 1 % EHEC, solid line - fitting line for 1 % EHEC. The EHEC 0.4 %, 0.6 % and 0.8% curves are time shifted.

25 % glycerol used in this study, which may account for the discrepancy in the measured relaxation times.

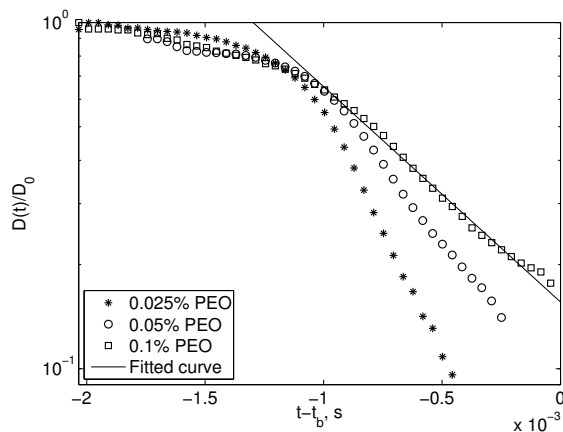


FIG. 9. The PEO filament thinning curve as a function of time,  $D(t)$ .  $*$  - 0.025 wt.% PEO,  $\circ$  - 0.05 wt.% PEO,  $\square$  - 0.1 wt.% PEO, solid line - curve fit for 0.1 wt.% PEO. Data for 0.025 wt.% PEO and 0.05 wt.% PEO solutions are timeshifted.

The values of  $\tau_E$  obtained from ROJER can be compared to the longest relaxation time estimated using the Rouse–Zimm model. This model is strictly valid only for dilute polymeric

solutions where  $c \ll c^*$ . For a mono-disperse polymer, the Zimm relaxation time,  $\tau_{Zimm}$ , is given by

$$\tau_{Zimm} = \frac{1}{\zeta(3\nu)} \frac{[\mu]\mu_s M_w}{RT} \quad (11)$$

where the front factor is approximated by  $\zeta$ , the Riemann zeta function,  $[\mu]$  is the intrinsic viscosity,  $R$  is the ideal gas constant and  $T$  the absolute temperature. The solvent quality factor,  $\nu$ , is estimated as 0.588 for EHEC [13], and  $\nu = 0.550$  for PEO [5]). Knowing the solvent quality parameter allows us to extract the intrinsic viscosity via the Mark-Houwink-Sakurada equation,

$$[\mu] = KM_w^{(3\nu-1)}, \quad (12)$$

where  $K$  is an empirical constant. For PEO in glycerol/water mixtures a value of  $K = 0.072$  has been established in the literature [27]. The  $K$  factor for EHEC is less reported, however Sharma et al. [13] reported a value of  $[\mu] = 388 \text{ cm}^3 \text{ g}^{-1}$  for an aqueous dispersion of EHEC with  $M_w \approx 2.4 \times 10^5 \text{ kg/kmol}$ , which would correspond to a value of  $K = 0.003$  for EHEC from Equation 12. Hence we can estimate the intrinsic viscosity,  $[\mu]$ , to be approximately  $261 \text{ cm}^3/\text{g}$  for our PEO and  $400 \text{ cm}^3/\text{g}$  for the EHEC respectively. These values are consistent with the shear viscosity measurements.

Using Equation 11 the Zimm relaxation time for the EHEC solutions is calculated to be  $\tau_{Zimm} = 61 \mu\text{s}$  compared to the extensional relaxation time of  $\tau_E = 139 \mu\text{s}$  obtained from ROJER for both the 0.4 and 0.6 % solutions. However, since  $c/c^* > 1$  these solutions are semi-dilute and therefore we would not expect the Rouse-Zimm theory to be valid. For the PEO solution the Zimm time is calculated to be  $\tau_{Zimm} = 43 \mu\text{s}$ . In this case,  $c/c^* \simeq 0.1 \ll 1$  so we expect the Rouse-Zimm model to hold, however, the relaxation time of  $\tau_E = 102 \mu\text{s}$  reported by ROJER is still significantly higher than the Zimm time. The difference is consistent with the observations of Tirtaatmadja et al. [27], where the relaxation times measured were substantially longer than the Zimm time, and found to be concentration dependent even for  $c/c^* \ll 1$ . Therefore the Zimm relaxation time is treated as a lower bound on the relaxation times measured in the ROJER experiments.

Instantaneous strain rate data is computed using the thinning curve,  $D(t)$ , together with Equation 6. Meaningful data is acquired for both EHEC and PEO solutions, examples of which are shown in Figures 10 and 11. Extension rates during the first and last stages of the thinning are noisy. This could be due to uneven lighting encountered at the top of the image, video conversion, and limited camera and lens resolution. Nevertheless, the curves follow behaviour observed by

Keshavarz et al. [12], where the extension rate approaches a plateau in the elastocapillary regime that corresponds to a critical strain rate of  $(2/3\tau_E)$ .

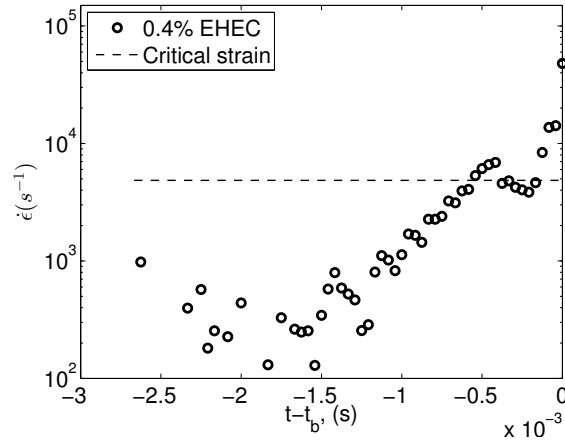


FIG. 10. The 0.4 wt.% EHEC strain rate over time ( $We = 21.95$ ,  $Oh = 0.065$ ). The dashed line denotes the critical strain rate,  $2/3\tau_E$ , ( $\circ$ ) - strain rate data.

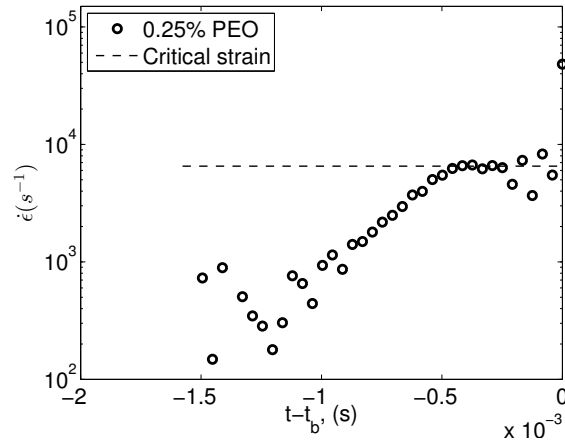


FIG. 11. The 0.025 wt.% PEO strain rate over time ( $We = 20.5$ ,  $Oh = 0.025$ ). The dashed line denotes the critical strain rate,  $2/3\tau_E$ , ( $\circ$ ) - strain rate data.

## V. COMPARISON OF THE ROJER AND CAPILLARY BRIDGE THINNING TECHNIQUES

The capillary thinning of the same range of PEO polymeric fluids were also measured using the Cambridge Trimaster apparatus [6]. These experiments also find a region of apparent elastocapillary thinning from which a relaxation time can be determined, given in Table III. Clearly, there is discrepancy between the two techniques with the Trimaster measurements being a factor of 2 to 3 times larger than found with ROJER. It is speculated that amongst the possible causes are:

- The Trimaster apparatus was operating at the limit of its capabilities. In particular when the movement of the pistons is ceased, the droplets attached to the piston oscillated due to the very low viscosity of the fluid. As a result, the thinning filament could have been affected by the subsequent slowing of break-up since fluid is forced back from the cusps into the liquid thinning bridge.

TABLE III. Comparisons of the relaxation times observed using the ROJER ( $\tau_{ER}$ ) and the Trimaster ( $\tau_{EC}$ ) for PEO solutions.

Polymer wt. %	$\tau_{ER}$ ( $\mu\text{s}$ )	$\tau_{EC}$ ( $\mu\text{s}$ )	$\tau_{EC}/\tau_{ER}$
PEO 0.025%	102	272	2.7
PEO 0.05%	165	366	2.2
PEO 0.1%	233	559	2.4

- The strain rates are different in the ROJER and Trimaster configurations, which could cause the observed discrepancy in the relaxation times. The ROJER technique uses a significantly smaller length scale controlled by the needle nozzle diameter ( $D_0 = 210\mu\text{m}$ ), whilst the Trimaster uses end-plates an order of magnitude larger.
- The initial strain rate history experienced by the polymers in the two experiments is quite different. In the Trimaster experiment, the polymers experience a rapid extensional flow as the endplates are separated, whereas in the ROJER experiment the polymers undergo a shear deformation as they are jetted through the nozzle. Clearly, further work is required to understand the impact of these deformations within the nozzle and resolve this discrepancy.
- Limitations of the current ROJER design. Image acquisition hardware and the image anal-

ysis method could be further improved, especially artefacts due to the pixel thresholding method, which are the subject of further studies now in progress.

## VI. CONCLUSIONS

A ROJER apparatus of a similar design to Keshavarz et al. [12] was assembled, but using a high speed camera rather than stroboscopic imaging to track the thinning filaments. The mechanical design was improved by implementing disposable needles in the nozzle design. This enables easy replacement if the needle becomes blocked, presenting a cheap and reliable nozzle design for testing complex fluids.

Thinning experiments were performed for Newtonian fluids for both the original orifice and the needle nozzle designs and the results compared with CFD simulations. The needle design produces a jet with a slightly smaller diameter than the nozzle as a consequence of the relaxation of the parabolic velocity profile. As a result, the critical perturbation frequency must be adjusted, but once this is accounted for, the needle nozzle gives the same results as the orifice design. Overall, a strong agreement was found between the CFD, orifice and needle nozzles. It was also found that a simple square wave signal could be used instead of the more complex sine wave function generator, provided that the perturbation frequency was the same, potentially simplifying the function generator hardware. These observations demonstrate that the ROJER apparatus is robust in its needle nozzle design and actuation drive signal.

The needle nozzle design was then used to characterise the capillary thinning of solutions of EHEC and PEO, with average molecular weights of  $M_w \approx 2.5 \times 10^5$  kg/kmol and  $M_w \approx 3 \times 10^5$  kg/kmol, respectively at various concentrations in a 25% glycerol and 75% water solvent. The measuring technique restricted the range of measurable relaxation times to between approximately 100 and 500  $\mu$ s due to need for the thinning to occur within the frame of the observation. This restriction limited the polymer concentrations for which a measurement of relaxation time can be measured. Strain rates were evaluated and confirmed that close to break-up, a constant critical value was approached, indicating that the elastocapillary balance was achieved. In all cases the observed relaxation time is significantly longer than the relaxation predicted from Zimm theory and remains concentration dependent even for polymer concentration well below  $c^*$ , in agreement with previously reported observations [27]. For the highest of the PEO concentrations measured, 0.1%, we obtained a relaxation of time of 233  $\mu$ s compared to a value of 360  $\mu$ s previously reported

[12] for the same polymer concentration, but in a more viscous solvent. However our measured relaxation times were significantly shorter than those obtained using the Cambridge Trimaster capillary thinning rheometer. These fluids are at lower limit for relaxation time measurement for this technique and so the ROJER device provides a viable alternative technique for characterise fast relaxing low viscosity fluids in extension.

## ACKNOWLEDGEMENTS

This work was supported by the Engineering and Physical Sciences Research Council (EPSRC) Centre for Doctoral Training in Fluid Dynamics at The University of Leeds under Grant No. EP/L01615X/1.

## REFERENCES

---

- [1] J. W. Hoyt, J. J. Taylor, and C. D. Runge. The structure of jets of water and polymer solution in air. *Journal of Fluid Mechanics*, 63(04):635–640, 1974.
- [2] F. T. Trouton. On the coefficient of viscous traction and its relation to that of viscosity. *Proceedings of the Royal Society of London. Series A, Containing Papers of a Mathematical and Physical Character*, pages 426–440, 1906.
- [3] G. H. McKinley. Visco-elasto-capillary thinning and break-up of complex fluids. *Rheology Reviews*, pages 1–48, 2005.
- [4] A.V. Bazilevsky, V.M. Entov, and A.N. Rozhkov. Liquid filament microrheometer and some of its applications. In *Third European Rheology Conference and Golden Jubilee Meeting of the British Society of Rheology*, pages 41–43. Springer, 1990.
- [5] L. E. Rodd, T. P. Scott, J. J. Cooper-White, and G. H. McKinley. Capillary break-up rheometry of low-viscosity elastic fluids. *Applied Rheology*, 15(1):12–27, 2005.
- [6] D. Vadillo, T. R. Tuladhar, A. C. Mulji, M. Mackley, S Jung, and S. D. Hoath. The development of the cambridge trimaster filament stretch and break-up device for the evaluation of ink jet fluids. *Journal of Rheology*, 54(2):261–282, 2010.

- [7] D. Vadillo, W. Mathues, and C. Clasen. Microsecond relaxation processes in shear and extensional flows of weakly elastic polymer solutions. *Rheologica acta*, 51(8):755–769, 2012.
- [8] D. T. Papageorgiou. On the breakup of viscous liquid threads. *Physics of Fluids*, 7(7):1529–1544, 1995.
- [9] J. Eggers. Universal pinching of 3D axisymmetric free-surface flow. *Physical Review Letters*, 71(21):3458, 1993.
- [10] J. Eggers. Nonlinear dynamics and breakup of free-surface flows. *Reviews of Modern Physics*, 69(3):865, 1997.
- [11] L. Campo-Deano and C. Clasen. The slow retraction method (SRM) for the determination of ultra-short relaxation times in capillary breakup extensional rheometry experiments. *Journal of Non-Newtonian Fluid Mechanics*, 165(23):1688–1699, 2010.
- [12] B. Keshavarz, V. Sharma, E. C. Houze, M. R. Koerner, J. R. Moore, P. M. Cotts, P. Threlfall-Holmes, and G. H. McKinley. Studying the effects of elongational properties on atomization of weakly viscoelastic solutions using rayleigh ohnesorge jetting extensional rheometry (ROJER). *Journal of Non-Newtonian Fluid Mechanics*, 222:171–189, 2015.
- [13] V. Sharma, S. J. Haward, J. Serdy, B. Keshavarz, A. Soderlund, P. Threlfall-Holmes, and G. H. McKinley. The rheology of aqueous solutions of ethyl hydroxy-ethyl cellulose (EHEC) and its hydrophobically modified analogue (hmEHEC): extensional flow response in capillary break-up, jetting (ROJER) and in a cross-slot extensional rheometer. *Soft matter*, 11(16):3251–3270, 2015.
- [14] J. B. Keller, S. Rubinow, and Y. Tu. Spatial instability of a jet. *Physics of Fluids*, 16:2052–2055, 1973.
- [15] J. Plateau. Ueber die gränze der stabilität eines flüssigen cylinders. *Annalen der Physik*, 156(8):566–569, 1850.
- [16] J. Eggers and E. Villermaux. Physics of liquid jets. *Reports on progress in physics*, 71(3):036601, 2008.
- [17] S. Middleman. Stability of a viscoelastic jet. *Chemical Engineering Science*, 20(12):1037–1040, 1965.
- [18] D. W. Bousfield, R. Keunings, G. Marrucci, and M. M. Denn. Nonlinear analysis of the surface tension driven breakup of viscoelastic filaments. *Journal of Non-Newtonian Fluid Mechanics*, 21(1):79–97, 1986.
- [19] C. Clasen, J. Eggers, M. A. Fontelos, J. Li, and G. H. McKinley. The beads-on-string structure of viscoelastic threads. *Journal of Fluid Mechanics*, 556:283–308, 2006.

- [20] V. M. Entov and E. J. Hinch. Effect of a spectrum of relaxation times on the capillary thinning of a filament of elastic liquid. *Journal of Non-Newtonian Fluid Mechanics*, 72(1):31–53, 1997.
- [21] F. Durst, S. Ray, B. Ünsal, and O. A. Bayoumi. The development lengths of laminar pipe and channel flows. *Journal of Fluids Engineering*, 127(6):1154–1160, 2005.
- [22] W. W. Graessley. Polymer chain dimensions and the dependence of viscoelastic properties on concentration, molecular weight and solvent power. *Polymer*, 21(3):258–262, 1980.
- [23] C. Clasen, J. P. Plog, W. M. Kulicke, M. Owens, C. Macosko, L. E. Scriven, M. Verani, and G. H. McKinley. How dilute are dilute solutions in extensional flows? *Journal of Rheology*, 50(6):849–881, 2006.
- [24] C. McIlroy. *Complex inkjets: particles, polymers and non-linear driving*. PhD thesis, University of Leeds, 2014.
- [25] ANSYS Inc. *ANSYS Fluent Theory Guide*. Ansys Inc., 2013.
- [26] S. Middleman and J. Gavis. Expansion and contraction of capillary jets of newtonian liquids. *Physics of Fluids*, 4(3):355–359, 1961.
- [27] V. Tirtaatmadja, G. H. McKinley, and J. J. Cooper-White. Drop formation and breakup of low viscosity elastic fluids: effects of concentration and molecular weight. *Physics of Fluids*, 18(4):043101, 2006.